DEVELOPMENT OF PRE-CLINICAL MURINE MODELS FOR FIBROLAMELLAR HEPATOCELLULAR CARCINOMA

Andy He[1,2*], Garry L. Coles[1,2*], Griffin G. Hartmann[1,2], Vicky Le[1,2], Brandon Mauch[1,2], Lei Xu[1,2], Thuyen Nguyen[1,2], Florette K. Hazard[1,3], and Julien Sage[1,2#]

Departments of [1]Pediatrics, [2]Genetics, and [3]Pathology, Stanford University School of Medicine, Stanford, CA, USA.

* Equal contribution

#Correspondence: julsage@stanford.edu

Authors Contributions: G.L.C. and J.S. designed the project together, with initial input from L.X.; G.L.C. performed most of the experiments related to characterizing the transgenic mice, with help from V.L., B.M., T.N., and A.H.; A.H. performed most of the experiments related to *ex vivo* culture assays and the drug treatment; F.K.H. performed histopathological analyses; G.G.H. analyzed the RNA sequencing data; G.L.C., A.H., G.G.H., and J.S. interpreted the experiments together; A.H., and J.S. wrote the manuscript and prepared the figures with contributions from all authors.

Keywords: fibrolamellar carcinoma, liver, cancer, PKA, organoids, mouse models

ABSTRACT

Fibrolamellar hepatocellular carcinoma (FLC) is a rare form of cancer that affects primarily adolescents and young adults. FLC tumors are typically associated with an intrachromosomal deletion resulting in expression of a fusion protein between the chaperone DNAJ1B and the protein kinase PKA. FLC is challenging to study because of its rarity and limited pre-clinical models. Here we developed a novel transgenic mouse model of FLC. In this model, DNAJ1B-PKA expression in the liver of mouse embryos results in perinatal lethality while DNAJ1B-PKA expression in the liver of adult mice initiates tumors resembling FLC at low penetrance. Some of these tumors can be serially propagated in 3D cultures and in allografts, including in syngeneic hosts. One such model shows growth inhibition upon treatment with the CDK4/6 inhibitor palbociclib. New pre-clinical models of FLC will provide novel insights into the biology of this rare cancer and may help identify novel therapeutic strategies.

INTRODUCTION

While hepatocellular carcinoma (HCC) in adults is a leading cause of mortality worldwide [1], liver cancer is much rarer in children and young adults. A majority of pediatric liver cancer cases are hepatoblastomas but primary HCCs are sometimes diagnosed [2]. In particular, fibrolamellar hepatocellular carcinoma (FL-HCC, or FLC) is a very rare and distinct subtype of HCC that affects adolescents and young adults. FLC develops in the setting of normal healthy livers, with no known genetic predisposition factor [3-5]. FLC is associated with better survival than HCC in adults, presumably due to the young age of the patients and the lack of cirrhosis, which makes more aggressive surgery possible [6]. However, few therapeutic options have been successfully explored beyond surgery. The 5-year survival rate ranges from 35-75% in patients treated with liver transplantation or resection. In cases where surgery is not possible, the survival drops to 12-14 months [7-10].

Morphologically, FLC tumors are characterized by pleomorphic malignant hepatocytes with large central nucleoli and abundant eosinophilic cytoplasm. The cancer cells are arranged in variably sized nests or cords set within a meshwork of lamellated collagen fibers. In the majority of cases, FLC cells contain hyaline droplets and some isolated cells have round cytoplasmic inclusions known as “pale bodies” [11, 12]. FLC express markers associated with biliary (e.g., CK7 and MUC1) and hepatocytic (e.g., Heppar-1, Albumin, α-1-antitrypsin, and Glypican-3) differentiation, as well as hepatic progenitor/stem cells (e.g., CK19, EPCAM) [3, 13-19].

At the genetic level, a breakthrough in the field was the discovery of a fusion event resulting in high levels of the catalytic subunit of PKA (protein kinase A) in FLC tumors [20, 21]. This finding was confirmed in other studies [22-24]. Rare cases of FLC have been associated with genetic inactivation of *PRKAR1A*, which encodes a regulatory subunit of PKA [25]. Rare cases of *BAP1* mutant HCC also have features of FLC and show amplification of the *PRKACA* gene coding for PKA with no fusion event [26]. Thus, high PKA activity may be sufficient to drive FLC development. Indeed, expression of PKA in the liver of young adult mice is sufficient to initiate tumors resembling FLC [27, 28]. In addition, inhibition of PKA kinase activity has anti-tumor activity against pre-clinical

models of FLC [29] and knock-down of the fusion protein inhibits the growth of patient-derived xenografts [30]. However, the small part of DNAJ1B fused to PKA in FLC tumors also contributes to tumor development in mice [27], an observation supported by biochemical and structural studies [31-36]. Few additional alterations have been found in the genome of FLC tumors, but accumulating evidence suggests a role for telomerase activity, MAPK signaling, and WNT signaling [26, 27, 35, 37-41].

The very low incidence rate of 0.02 per 100,000 has kept FLC an understudied cancer [42]. Very few cell lines and patient-derived xenograft models remain available, and these models often do not propagate easily, even though they can provide important model systems [16, 43, 44]. Similarly, mouse models have also been developed using CRISPR/Cas9 approaches; in these models, tumors recapitulate some key features of human FLC, but they grow slowly, limiting their use [27, 28]. Organoids derived from tumors have only been recently described [45, 46]. Here we engineered a new mouse allele in which the DNAJ1B-PKA fusion can be induced following Cre-mediated recombination in transgenic mice. We used this new model to investigate the consequences of DNAJ1B-PKA expression in the adult liver. We were able to develop allografts and 3D culture systems that are amenable to investigations exploring further the biology of FLC and identifying new therapeutic approaches.

RESULTS

Transgenic mice expressing DNAJ1B-PKA

We generated transgenic mice by inserting a *DNAJB1-PRKACA-GFP* cDNA into the *Rosa26* locus. Upon Cre-mediated recombination and self-cleaving of the fusion protein, this construct allows expression of the DNAJB1-PKA fusion found in human FLC and the GFP reporter (**Fig. 1A**). *Rosa26*$^{LSL\text{-}DNAJB1\text{-}PKA}$ transgenic mice were healthy and fertile, as would be expected for a conditional allele.

The cell of origin of FLC cannot be determined conclusively from patients. While mouse models have shown that adult hepatocytes can initiate FLC [27, 28], the development of FLC in young patients and the expression of stem cell markers in these tumors [3, 13-17, 44] are also suggestive of an initiating event early in liver development. We wondered if expression of the DNAJB1-PKA fusion in the developing liver may initiate FLC more frequently and more rapidly than in the adult setting. To test this idea, we crossed *Rosa26*$^{LSL\text{-}DNAJB1\text{-}PKA\text{-}GFP}$ mice to *Alb-Cre* mice where the Cre recombinase is expressed under the control of the *Albumin* promoter and is turned on at mid-gestation in the liver. Analysis of GFP expression showed positive signal in the liver of mice also expressing Cre at day E18.5 (**Fig. 1B**). Accordingly, we detected increased expression of *PRKACA* mRNA molecules in transgenic mice expressing Cre at the same time point (**Fig. 1C**). These observations indicated proper expression of the transgene and led us to investigate the consequences of DNAJB1-PKA expression in the embryonic liver for possible tumor development later in adult mice. However, no *Alb-Cre*;*Rosa26*$^{LSL\text{-}DNAJB1\text{-}PKA\text{-}GFP}$ pups from this cross survived past weaning (**Fig. 1D**). While the cause underlying this perinatal death is not known, these observations provided an initial validation of this new transgenic model to express the DNAJB1-PKA fusion in the liver of mice.

DNAJ1B-PKA expression in the adult liver of mice results in the development of slow-growing tumors with low penetrance

Fluorescence in situ hybridization (FISH) shows that the gene fusion is only present in FLC cells and not in surrounding liver cells [47]. To introduce the oncogenic fusion in a subset of adult liver cells and allow for clonal growth, we performed hydrodynamic tail

vein tail injections of *Rosa26*$^{LSL\text{-}DNAJB1\text{-}PKA\text{-}GFP}$ mice with a plasmid expressing the Cre recombinase (**Fig. 2A**), generating a cohort of 38 animals (28 males and 10 females). We aged these mice and waited for signs of disease before analysis. We found that 10 mice developed tumors (3 spleen tumors, which were not further studied, and 7 liver tumors – **Table S1** and **Fig. 2B**). The low penetrance of FLC development and the slow growth of these tumors in this transgenic model is consistent with previously described mouse models [27, 28], and makes it difficult to use these mice as pre-clinical models of FLC development and response to candidate therapies.

We thus wondered if some of the most aggressive tumors in transgenic mice may be able to be transplanted into recipient mice in allograft models. We were able to generate single-cell suspensions from tumors in 5 out 7 of the mice with liver tumors, 2 of which grew in NSG immunodeficient mice upon subcutaneous injection. One allograft model had a fibrosarcoma histology and was not pursued further (**Fig. S1A,B**). The other tumor, FL1 (shown in **Fig. 2B**), had histopathological features of FLC and some GFP expression by immunostaining (**Fig. S1C,D**); the first allograft generated from this primary tumor stopped growing when its size was still small and did not further expand in subsequent passages, and it was not further studied.

Based on this low efficiency of tumor take from single cells, we also directly implanted small pieces from 2/7 tumors subcutaneously into NSG mice. These two models, FL2 and FL8, grew and could be propagated into new NSG hosts. Cells in these tumors were positive for the liver marker HNF4α (Hepatocyte nuclear factor 4α) [48] and GFP (**Fig. 2C** and **Fig. S2A**). Similar to the two other mouse models previously described [27, 28], FL2 and FL8 tumors were largely negative for the expression of cytokeratins 17 and 19 (CK17/19) (**Fig. S2B**). These same two mice had lung metastases (**Fig. S2C**), which we also microdissected to generate two additional models, FL2M and FL8M, which were expanded in NSG mice. For FL2 and FL8, tumor growth was slow and variable, from 3-6 months, but these tumors retained their initial histology (**Fig. 2D-H**).

We attempted to grow FL2 and FL8 cells into immunocompetent mice (n=3 tumor pieces for FL2 and FL8, n=5 each for FL2 and FL8 for cell suspensions). To increase the probability that some of the cancer cells may grow, we performed orthotopic

transplantations: for both FL2 and FL8, we sutured tumor fragments into the liver of 3 mice per line, and injected cell suspensions into the liver of 5 mice per line. We chose F1 mice between pure C57BL/6 and 129Sv/J to recapitulate the MHC alleles in the *Rosa26*$^{LSL\text{-}DNAJB1\text{-}PKA\text{-}GFP}$ mice (which are in a mixed background between these two mouse strains). Both the FL2 and the FL8 models grew in the liver of F1 hosts upon injection of sutured tumor fragments (**Fig. 2I,J** and **Fig. S2D,E**).

Overall, the development of liver tumors in this mouse model is slow and has low penetrance but FLC allografts derived from our transgenic mice can be serially passaged.

3D culture models for mouse FLC tumors

In the past few years, the development of 3D culture systems has enabled the analysis of normal tissues and tumors *ex vivo* under conditions more similar to *in vivo* conditions than 2D cultures. Human liver organoids have recently been described from human FLC tumors [45, 46]. We found that mouse FLC cells could be isolated from allografts and grown in 3D organoids in an air-liquid interface (ALI) system (**Fig. S3A**). However, these cells did not expand beyond 3 passages in this context (~1 passage per month), suggesting that these culture conditions are not optimal. Still, we were able to re-inject FL2 and FL8 cells from passages 2 and 1, respectively, in ALI organoids using orthotopic injections (cell suspensions) into the liver of NSG mice (**Fig. S3B**) (we chose orthotopic injections because of failure to grow from single cell suspensions in subcutaneous injections). The resulting allografts had retained FLC histology (**Fig. S3C**), indicating that *ex vivo* culture followed by re-implantation is possible for these models.

The growth of FLC allografts can be inhibited by palbociclib treatment

While FLC cells could grow orthotopically, tumor development was variable and unreliable in this assay. We sought to develop a subcutaneous model in which tumor initiation and tumor growth may be more consistent than single cell injections (rare tumor growth) and injections of tumor fragments (reliable tumor growth but variable growth rate). We wondered if a matrix that could recapitulate the stiffness of the liver microenvironment may provide a better environment for FLC cells to grow, as observed in other experiments to grow liver cells in 3D models [49-52]. We embedded mouse FLC cells in methacrylated gelatin (GelMA). GelMA is a biocompatible matrix with modular mechanical properties

[53] and it is compatible with the growth of liver epithelial cells [54]. FLC cells grew in GelMA (**Fig. 3A**) and FL8 cells embedded in GelMA were implanted subcutaneously in recipient mice (**Fig. 3A**) We found that tumor development was not visibly different between this method and the implantation of tumor fragments (compare controls in **Fig. S3D** to tumor growth **Fig. 2E,G**), but reproducible enough to perform a treatment experiment. We observed a mild tumor inhibitory effect of the CDK4/6 inhibitor palbociclib in this experiment (**Fig. 3C** and **Fig. S3D**).

We performed bulk RNA sequencing (RNA-seq) of tumors at the end of the experiment. When we analyzed the expression of genes that have been used as markers of FLC and other liver tumors (**Fig. 3D**), we found that the FL8 model in this context expressed genes such as *Alb* (coding for albumin), *Arg1* (coding for Arginase-1), *Krt8/18* (coding for cytokeratins 8 and 18), or *Serpin1a/b* (coding for Alpha-1-Antitrypsin) as expected for a liver cancer originating from hepatocytes [18, 55, 56]. Detection of *Krt5* (coding for cytokeratin 5) and *Muc1* (coding for Mucin1) in this analysis was more indicative of bile duct differentiation and could be a sign of dedifferentiation [14, 57]. Accordingly, expression of *Afp* (coding for Alpha-fetoprotein) was high in the FL8 model, and is a feature of FLC tumors with a worse prognosis [58, 59]. Expression of *Fgb* is a marker of FLC, with the encoded protein Fibrinogen B being present in pale bodies characteristic of this cancer type [55]. Palbociblib has recently be shown to promote differentiation in neuroblastoma [60], but we did not observe any significant changes in the expression of these “liver” genes in response to palbociclib (**Fig. 3D**). When we analyzed up- and down-regulated genes in tumors treated with palbociclib compared to controls, we found very few genes (n=8) with a significantly different expression (p-adj<0.05) between controls and palbociclib-treated tumors (**Table S2**). When we performed a gene ontology (GO) enrichment analysis of the 952 genes differentially expressed between the two conditions (p-value ≤0.05), we found an enrichment for cell cycle terms, as would be expected for treatment with a cell cycle inhibitor (**Fig. 3E** and **Table S3**) Overall, this analysis further supports that FL8 cells may represent an FLC-like model and suggests that FLC tumors may respond to CDK4/6 inhibitors such as palbociclib.

DISCUSSION

Here we present a new transgenic mouse model for human FLC based on expression of the DNAJ1B-PKA fusion protein. While a limitation of this mouse model is the low frequency and the slow development of tumors, these limitations can be in part circumvented by the expansion *ex vivo* of cell models derived from these tumors.

The *Rosa26*$^{LSL\text{-}DNAJB1\text{-}PKA}$ transgenic model is versatile as Cre can be delivered at different times and in different cell types using other mouse alleles or viral vectors. When we activated DNAJ1B-PKA during embryonic liver development, mice did not survive to adulthood, suggesting that expression of the fusion protein at this stage is detrimental to some aspect of liver function. This issue could be possibly alleviated by decreasing the number of liver cells expressing Cre and may help initiate tumors more efficiently than Cre delivery in the adult liver, for example using an *Alb-CreER* allele with tamoxifen-inducible Cre expression [61], using low doses of tamoxifen during embryogenesis. The *Rosa26*$^{LSL\text{-}DNAJB1\text{-}PKA}$ transgenic model could also be used to model other cancer types in which DNAJ1B-PKA is thought to be oncogenic, including rare cases of pancreatic cancer [62], which may be modeled using the appropriate Cre driver.

A growing number of organoid and patient-derived xenograft models are being developed from patients with FLC to investigate key features of this disease (see [29, 30, 45, 46, 63-66] for recent examples). We describe the growth of mouse FLC-like cell models in culture and as allografts. These murine models, which grow in immunocompetent hosts as primary tumors or allografts, may prove useful in the future to investigate specific aspects of FLC biology, including for example how these tumors interact with immune cells. We note that one possible limitation of our transgenic model is the expressing of GFP together with the fusion protein, as GFP is immunogenic [67]; this may confound some analyses focusing on the response of immune cells to cancer cells expressing DNAJ1B-PKA in this context. Mouse models also provide a simpler genetic setting to explore mechanisms of tumorigenesis, and it would be interesting in the future to determine how expression of the fusion protein in mouse hepatocytes or in cell models such as FL2 and FL8 or their metastatic derivatives FL2M and FL8M affects the biology of these cells compared to recent observations made in human models [34, 68].

We chose palbociclib as a proof-of-principle compound because genomic analyses of FLC tumors indicate that these tumors are wild-type for the *RB1* gene (coding for the RB tumor suppressor) [20-24] and our transgenic model was also engineered to be wild-type for *Rb1*. CDK4/6 inhibitors are approved for the treatment of breast cancer and presence of RB is required for tumor inhibition [69, 70]. The anti-tumor effects observed with the FL8 model were not very strong, which is possibly due to the fact that FL8 tumors do not expand very fast in the context studied. Future experiments may combine CDK4/6 inhibitors with other strategies such as chemotherapy or radiotherapy to induce more potent tumor inhibition.

It has often been difficult for rare diseases such as FLC to benefit from new therapies because pre-clinical models often lag compared to more frequent tumor types. The development of new mouse models, but also fish models [71], may help provide pre-clinical data that lead to the design of new clinical trials in patients with FLC.

Methods

Mice and generation of tumors

Mice were maintained according to practices prescribed by the NIH at Stanford's Research Animal Facility (approved protocol #32398). Additional accreditation of Stanford animal research facilities was provided by the Association for Assessment and Accreditation of Laboratory Animal Care (AAALAC).

A *Rosa26*$^{LSL\text{-}DNAJB1\text{-}PKA\text{-}GFP}$ C56BL/6 founder mouse was generated and validated by Applied StemCell using a site-specific integrase via pronuclear injection [72]. *Alb-Cre* mice were described before [73] and obtained from the Jackson Laboratory (Stock No: 035593). Primers for genotyping are available upon request.

To generate tumors in the liver of mice, 10-16-week-old mice were anesthetized using isoflurane, the tail vein was dilated with a heat pad, and 10 µg of Turbo-Cre plasmid was delivered in a solution of sterile PBS using a hydrodynamic tail-vein injection protocol. The Turbo-Cre plasmid was a gift from the laboratory of Dr. Steven Artandi at Stanford University. Mice were housed for 1-2 years before subsequent analysis.

RT-qPCR

Liver tissue was isolated by microdissection, minced with a razor blade, and total RNA was collected using RNeasy Fibrous Tissue Mini Kit (Qiagen). cDNA synthesis was performed using the iScript cDNA synthesis kit (Bio-Rad) and RT-qPCR was performed using iQ SYBRGreen supermix (Bio-Rad). The following RT-qPCR primers were used DNAJPRKACA F: 5'-TTACTACCAGACGTTGGGCCT-3', DNAJPRKACA R: 5'-ATAGTGGTTCCCGGTCTCCT-3', mPRKACA-aF: 5'-AGATCGTCCTGACCTTTGAGT-3', mPRKACA-aR: 5'-GGCAAAACCGAAGTCTGTCAC-3', mPRKACA-bF: 5'-GGTGACAGACTTCGGTTTTGC-3', mPRKACA-bR: 5'-CACAGCCTTGTTGTAGCCTTT-3'.

Immunostaining

Tissues were fixed with 4% paraformaldehyde (PFA) in phosphate-buffered saline (PBS). Liver tissues (normal or tumor) were initially perfused with 10 mL PFA through the inferior

vena cava. All tissues were submerged in 4% PFA for 48 hr before being switched to 70% ethanol and finally processed and embedded. Slides were deparaffinized in 2x 5 min changes of Histo-Clear (National Diagnostics HS-202), and rehydrated in 2x 1 min changes of 100% ethanol, 2x 1 min changes of 70% ethanol, and finally 2x 5 min changes of distilled water. Antigen retrieval was performed in a microwave for 10 min with citrate-based buffer (Vector Labs H-3300). Slides were cooled at room temperature, quenched for endogenous enzyme activity (SP-6000), and washed in 3x 3 min changes of PBS with 0.1% Tween-20 (PBST) (Sigma P1379). Slides were blocked with secondary antibody serum for 1 hr at room temperature (RT). GFP antibody (Cell Signaling Technology #2956) was diluted to 1:200 in PBST and applied to slides for 1 hr at 37 ºC. Slides were washed in 3x 3 min changes of PBST. Horse anti-rabbit secondary (Vector Labs MP-7401) was applied to slides for 1 hr at 37 ºC. Slides were washed in 3x 3 min changes of PBST. The chromogen was developed using a DAB substrate kit (Vector SK-4100) for 5 min before quenching in distilled water for 5 min. Slides were counterstained with hematoxylin (Newcomer Supply 1201B, dehydrated in 2x 1 min changes of 70% ethanol, 2x 1 min changes of 100% ethanol, and finally cleared in 2x 5 min changes of xylene before mounting.

Embryos were dissected from timed pregnant females, fixed in 4% PFA overnight and sections were generated as described above. Sections were depaffarinized, rehydrated, and tissue was blocked in 5% goat serum for 1 hr. Anti-GFP was added overnight. The following day, samples were washed before incubation with Goat anti-Rabbit - Alexa Fluor™ 488 (Thermo Fisher) and DAPI (Sigma). Samples were washed and mounted in ProLong Gold mounting media (Thermo Fisher) before confocal imaging.

Tumor transplantation studies

Nod.Cg-Prkdc^{scid}IL2rg^{tm1Wjl}/SzJ (NSG) mice (Jackson Laboratories, Stock No: 005557) were used for all experiments in immunodeficient recipients. For experiments in immunocompetent hosts, F1 mice between pure C57BL/6 and 129Sv/J were used (Jackson Laboratories, B6129SF1/J Stock No: 101043).

Tumors from *Rosa26*$^{LSL\text{-}DNAJB1\text{-}PKA\text{-}GFP}$ mice were microdissected from livers or lungs. Tumors were bisected once to increase surface area exposed to transplant media

(Kubota's medium) and kept on ice until ready for transplant. Recipient mice were anesthetized and shaved in the flank. The shaved flank was sterilized with one swab of betadine, one swab of 70% ethanol repeated 3 times. After confirming adequate depth of anesthesia by toe-pinch, a 5 mm incision was made in the shaved flank. Blunt dissection under the skin was used to separate the skin from the muscle, creating a pocket between the 2 layers. Tumor pieces were implanted (bisected side facing the muscular wall, ~5 mm piece) near macroscopically visible capillaries on muscle wall. The incision was closed using 9 mm wound clips. For subcutaneous tumors, tumor volume was calculated following this formula:

$$Tumor\ Volume = \frac{4}{3}\pi\left(\frac{L+W}{4}\right)^3$$

Cell Culture

Allografts were minced into 1-2 mm^3 fragments and incubated for 10 min at 37 ºC in an enzymatic cocktail of Collagenase 1 (0.85 mg/mL, Sigma C0130) Collagenase 2 (0.28 mg/mL, Sigma C6885), Collagenase IV (0.85 mg/mL, Sigma 5138), Elastase (0.125 mg/mL Worthington LSL002292), DNAse 1 (0.125 mg/mL Roche 1014159001) in L-15 Medium (Sigma L1518).

To generate organoids, cells were pelleted and resuspended in Matrigel (Fisher 356213) at 10^4-10^5 cells/mL. One volume of Matrigel with no cells was pipetted into a transwell insert to gel at 37 ºC for 10 min. One volume of Matrigel with cell suspension was pipetted onto the top of the acellular Matrigel layer and incubated for an additional 10 min at 37 ºC. Kubota's Medium (Phoenix Songs Biologicals 35101) was added outside the transwell to a volume that submerged the acellular Matrigel layer and but left the cellular layer exposed to air. Cells were fed 3 times a week for 1-2 months.

To passage cells, wells were washed 3x with PBS. Matrigel layers were collected into a 50 mL conical and incubated with an equivalent volume of Cell Recovery Solution (Corning 354253). Layers and Recovery solution were incubated at 4 ºC for 30 min with vigorous pipetting every 5 min. Cells were pelleted and resuspended in Matrigel for following passages.

For GelMA experiments, 20% w/v Gelatin (Sigma G1890) in 0.25 M carbonate-bicarbonate (CB) buffer was mixed with methacrylic anhydride (MA) (Thermo Fisher 760-93-0) at 0.1mL/1g MA to gelatin for 1 hr at 37 ºC. This solution was henceforth referred to as GelMA. Unreacted MA was removed by spinning solution at 3500 g for 5 min at RT. Supernatant was collected with unreacted MA pellet discarded. GelMA was diluted three-fold and dialyzed in 10 K MWCO tubing (Thermo Fisher 88245) for 7 days at 37 ºC against Milli-Q water. Water was changed twice a day. Dialyzed GelMA was frozen at -80 ºC overnight before lyophilization. Lyophilized GelMA was reconstituted at 20% w/v in RPMI, 0.005 N NaOH, 20 mM HEPES, 0.22 g $NaHCO_3$, and sterile filtered with 0.45 µm filters. To embed cells in GelMA, 20% w/v aliquots of GelMA were diluted 1:2 with RPMI to form 10% w/v solution. Cells were resuspended at appropriate concentrations. Lithium phenyl-2,4,6-trimethylbenzoylphosphinate (LAP) (Sigma 900889) was mixed into solution to final concentration of 0.67% w/v LAP. Gel was crosslinked with 405 nm light for 3 min.

Orthotopic Injection and Implantation

To generate tumors, cells were disaggregated from Matrigel using the protocol described above**.** Cell pellets were resuspended at a concentration of 10^4-10^5 cells in 25 µL. These cell suspensions were mixed with an equivalent volume of Matrigel to a total volume of 50 µL. Mice were anesthetized and shaved in the abdomen. Lateral incision was made in the skin directly inferior to xyphoid process. Blunt dissection was used to separate surrounding skin from parenchyma and musculature. Incision was made in caudal direction originating from xyphoid process. The largest liver lobe available was exposed and stabilized. For cell injection, 20 µL of cells mixed 1:1 with Matrigel were injected. For tissue implantation, tissue 3-8 mm-wide at longest axis was sutured to the liver lobe using 5-0 vicryl suture. Liver lobe was returned to original site. Mouse musculature was closed with 5-0 vicryl running suture, skin was closed with 9mm wound clips.

Drug Study

FL8 cells were suspended at concentration of 10^6 cells/100 µL in 10% w/v methacrylated gelatin (Sigma 276685) and 0.067% w/v LAP (Sigma 900889) suspended in RPMI (Sigma R0883). 200 µL aliquots in 96-well plates were photo-crosslinked into solid capsules at

405 nm light (Amazon 0191673174324) for 3 min at room temperature. Capsules were implanted in the subcutaneous flanks of NSG mice. When average tumor size reached 75 mm^3 mice were randomized into treatment groups. Mice either received vehicle (0.5% methocel Sigma 94378) or palbociclib (LC Laboratories P-7788) at a dose of 75 mg/kg via oral gavage for 3 consecutive days and given 4 days with no treatment.

RNA sequencing analysis

Frozen tumor samples were sent to Novogene for RNA extraction and library preparation. Raw sequencing reads were demultiplexed by the vendor to generate approximately 20 million paired-end reads per sample. Fastq files were trimmed using CutAdapt (v2.10) [74] using TruSeq sequencing adapter (5'-AGATCGGAAGAGCACACGTCTGAACTCCAGTCAC-3'), and a minimum read length of at least 25. Reads were then aligned to the ENSEMBL mm10 genome using HiSat2 [75] using reverse strandedness and discarding unaligned reads. Counts were assigned to genes using featureCounts [76] at ENSEMBL gene annotation (v93). Differential expression analysis was conducted using DESeq2 [77] on R v4.1.2 (https://www.R-project.org/).

Statistics and reproducibility

Statistical significance was assessed using the Prism GraphPad software. The specific tests used are indicated in the figure legends. Mice for *in vivo* studies were randomized where applicable and sample sizes determined by pilot experiments or previous experiments using similar models. Investigators were not blinded to allocation during experiments and outcome assessment.

Data availability

All RNA sequencing datasets generated in this study are available at Gene Expression Omnibus (GEO) under Super Series GSE249325 (https://www.ncbi.nlm.nih.gov/geo/query/acc.cgi?acc=GSE249325). All other data are available in the article and supplementary materials, or from the corresponding author upon reasonable request.

Acknowledgments

We thank Pauline Chu from the histology facility for her help with tissue sections and all the members of the Sage lab for their help and support throughout this study. Research reported in this publication was supported by grants from the Fibrolamellar Cancer Foundation, the Alex's Lemonade Stand Foundation, and the National Cancer Institute (CA228413). J.S. is the Elaine and John Chambers Professor in Pediatric Cancer.

REFERENCES

1. Yang JD, Hainaut P, Gores GJ, Amadou A, Plymoth A, Roberts LR. A global view of hepatocellular carcinoma: trends, risk, prevention and management. Nat Rev Gastroenterol Hepatol. 2019;16(10):589-604. Epub 2019/08/24. doi: 10.1038/s41575-019-0186-y. PubMed PMID: 31439937; PubMed Central PMCID: PMCPMC6813818.

2. Ranganathan S, Lopez-Terrada D, Alaggio R. Hepatoblastoma and Pediatric Hepatocellular Carcinoma: An Update. Pediatr Dev Pathol. 2020;23(2):79-95. Epub 2019/09/27. doi: 10.1177/1093526619875228. PubMed PMID: 31554479.

3. Ward SC, Waxman S. Fibrolamellar carcinoma: a review with focus on genetics and comparison to other malignant primary liver tumors. Semin Liver Dis. 2011;31(1):61-70. Epub 2011/02/24. doi: 10.1055/s-0031-1272835. PubMed PMID: 21344351.

4. Chakrabarti S, Tella SH, Kommalapati A, Huffman BM, Yadav S, Riaz IB, et al. Clinicopathological features and outcomes of fibrolamellar hepatocellular carcinoma. J Gastrointest Oncol. 2019;10(3):554-61. Epub 2019/06/12. doi: 10.21037/jgo.2019.01.35. PubMed PMID: 31183207; PubMed Central PMCID: PMCPMC6534717.

5. O'Neill AF, Church AJ, Perez-Atayde AR, Shaikh R, Marcus KJ, Vakili K. Fibrolamellar carcinoma: An entity all its own. Curr Probl Cancer. 2021;45(4):100770. Epub 20210701. doi: 10.1016/j.currproblcancer.2021.100770. PubMed PMID: 34272087.

6. Njei B, Konjeti VR, Ditah I. Prognosis of Patients With Fibrolamellar Hepatocellular Carcinoma Versus Conventional Hepatocellular Carcinoma: A Systematic Review and Meta-analysis. Gastrointest Cancer Res. 2014;7(2):49-54. Epub 2014/05/07. PubMed PMID: 24799971; PubMed Central PMCID: PMCPMC4007676.

7. Stevens WR, Johnson CD, Stephens DH, Nagorney DM. Fibrolamellar hepatocellular carcinoma: stage at presentation and results of aggressive surgical management. AJR Am J Roentgenol. 1995;164(5):1153-8. Epub 1995/05/01. doi: 10.2214/ajr.164.5.7717223. PubMed PMID: 7717223.

8. Katzenstein HM, Krailo MD, Malogolowkin MH, Ortega JA, Qu W, Douglass EC, et al. Fibrolamellar hepatocellular carcinoma in children and adolescents. Cancer. 2003;97(8):2006-12. Epub 2003/04/04. doi: 10.1002/cncr.11292. PubMed PMID: 12673731.

9. Ang CS, Kelley RK, Choti MA, Cosgrove DP, Chou JF, Klimstra D, et al. Clinicopathologic characteristics and survival outcomes of patients with fibrolamellar carcinoma: data from the fibrolamellar carcinoma consortium. Gastrointest Cancer Res. 2013;6(1):3-9. Epub 2013/03/19. PubMed PMID: 23505572; PubMed Central PMCID: PMCPMC3597938.

10. Chun YS, Zimmitti G. Fibrolamellar variant of hepatocellular carcinoma. Recent Results Cancer Res. 2013;190:101-10. Epub 2012/09/04. doi: 10.1007/978-3-642-16037-0_7. PubMed PMID: 22941016.

11. Craig JR, Peters RL, Edmondson HA, Omata M. Fibrolamellar carcinoma of the liver: a tumor of adolescents and young adults with distinctive clinico-pathologic features. Cancer. 1980;46(2):372-9. Epub 1980/07/15. doi: 10.1002/1097-0142(19800715)46:2<372::aid-cncr2820460227>3.0.co;2-s. PubMed PMID: 6248194.

12. Liu S, Chan KW, Wang B, Qiao L. Fibrolamellar hepatocellular carcinoma. Am J Gastroenterol. 2009;104(10):2617-24; quiz 25. Epub 2009/07/30. doi: 10.1038/ajg.2009.440. PubMed PMID: 19638962.

13. Yamashita T, Forgues M, Wang W, Kim JW, Ye Q, Jia H, et al. EpCAM and alpha-fetoprotein expression defines novel prognostic subtypes of hepatocellular carcinoma. Cancer Res. 2008;68(5):1451-61. Epub 2008/03/05. doi: 10.1158/0008-5472.CAN-07-6013. PubMed PMID: 18316609.

14. Ward SC, Huang J, Tickoo SK, Thung SN, Ladanyi M, Klimstra DS. Fibrolamellar carcinoma of the liver exhibits immunohistochemical evidence of both hepatocyte and bile duct differentiation. Mod Pathol. 2010;23(9):1180-90. Epub 2010/05/25. doi: 10.1038/modpathol.2010.105. PubMed PMID: 20495535.

15. Ross HM, Daniel HD, Vivekanandan P, Kannangai R, Yeh MM, Wu TT, et al. Fibrolamellar carcinomas are positive for CD68. Mod Pathol. 2011;24(3):390-5. Epub 2010/11/30. doi: 10.1038/modpathol.2010.207. PubMed PMID: 21113139; PubMed Central PMCID: PMCPMC3292186.

16. Oikawa T, Kamiya A, Zeniya M, Chikada H, Hyuck AD, Yamazaki Y, et al. Sal-like protein 4 (SALL4), a stem cell biomarker in liver cancers. Hepatology. 2013;57(4):1469-83. Epub 2012/11/24. doi: 10.1002/hep.26159. PubMed PMID: 23175232; PubMed Central PMCID: PMCPMC6669886.

17. Van Eyken P, Sciot R, Brock P, Casteels-Van Daele M, Ramaekers FC, Desmet VJ. Abundant expression of cytokeratin 7 in fibrolamellar carcinoma of the liver. Histopathology. 1990;17(2):101-7. Epub 1990/08/01. doi: 10.1111/j.1365-2559.1990.tb00679.x. PubMed PMID: 1699871.

18. Berman MA, Burnham JA, Sheahan DG. Fibrolamellar carcinoma of the liver: an immunohistochemical study of nineteen cases and a review of the literature. Hum Pathol. 1988;19(7):784-94. doi: 10.1016/s0046-8177(88)80261-2. PubMed PMID: 2456977.

19. Alshareefy Y, Shen CY, Prekash RJ. Exploring the molecular pathogenesis, diagnosis and treatment of fibrolamellar hepatocellular carcinoma: A state of art review of the current literature. Pathol Res Pract. 2023;248:154655. Epub 20230626. doi: 10.1016/j.prp.2023.154655. PubMed PMID: 37429175.

20. Honeyman JN, Simon EP, Robine N, Chiaroni-Clarke R, Darcy DG, Lim, II, et al. Detection of a recurrent DNAJB1-PRKACA chimeric transcript in fibrolamellar hepatocellular carcinoma. Science. 2014;343(6174):1010-4. Epub 2014/03/01. doi: 10.1126/science.1249484. PubMed PMID: 24578576; PubMed Central PMCID: PMCPMC4286414.

21. Simon SM. Fighting rare cancers: lessons from fibrolamellar hepatocellular carcinoma. Nature Reviews Cancer. 2023;23(5):335-46.

22. Cornella H, Alsinet C, Sayols S, Zhang Z, Hao K, Cabellos L, et al. Unique genomic profile of fibrolamellar hepatocellular carcinoma. Gastroenterology. 2015;148(4):806-18 e10. Epub 2015/01/06. doi: 10.1053/j.gastro.2014.12.028. PubMed PMID: 25557953; PubMed Central PMCID: PMCPMC4521774.

23. Xu L, Hazard FK, Zmoos AF, Jahchan N, Chaib H, Garfin PM, et al. Genomic analysis of fibrolamellar hepatocellular carcinoma. Hum Mol Genet. 2015;24(1):50-63. Epub 2014/08/15. doi: 10.1093/hmg/ddu418. PubMed PMID: 25122662; PubMed Central PMCID: PMCPMC4262492.

24. Graham RP, Jin L, Knutson DL, Kloft-Nelson SM, Greipp PT, Waldburger N, et al. DNAJB1-PRKACA is specific for fibrolamellar carcinoma. Mod Pathol. 2015;28(6):822-9. Epub 2015/02/24. doi: 10.1038/modpathol.2015.4. PubMed PMID: 25698061.

25. Graham RP, Lackner C, Terracciano L, Gonzalez-Cantu Y, Maleszewski JJ, Greipp PT, et al. Fibrolamellar carcinoma in the Carney complex: PRKAR1A loss instead of the classic

DNAJB1-PRKACA fusion. Hepatology. 2018;68(4):1441-7. Epub 2017/12/10. doi: 10.1002/hep.29719. PubMed PMID: 29222914; PubMed Central PMCID: PMCPMC6151295.

26. Hirsch TZ, Negulescu A, Gupta B, Caruso S, Noblet B, Couchy G, et al. BAP1 mutations define a homogeneous subgroup of hepatocellular carcinoma with fibrolamellar-like features and activated PKA. J Hepatol. 2020;72(5):924-36. Epub 2019/12/22. doi: 10.1016/j.jhep.2019.12.006. PubMed PMID: 31862487.

27. Kastenhuber ER, Lalazar G, Houlihan SL, Tschaharganeh DF, Baslan T, Chen CC, et al. DNAJB1-PRKACA fusion kinase interacts with beta-catenin and the liver regenerative response to drive fibrolamellar hepatocellular carcinoma. Proc Natl Acad Sci U S A. 2017;114(50):13076-84. Epub 2017/11/23. doi: 10.1073/pnas.1716483114. PubMed PMID: 29162699; PubMed Central PMCID: PMCPMC5740683.

28. Engelholm LH, Riaz A, Serra D, Dagnaes-Hansen F, Johansen JV, Santoni-Rugiu E, et al. CRISPR/Cas9 Engineering of Adult Mouse Liver Demonstrates That the Dnajb1-Prkaca Gene Fusion Is Sufficient to Induce Tumors Resembling Fibrolamellar Hepatocellular Carcinoma. Gastroenterology. 2017;153(6):1662-73 e10. Epub 2017/09/20. doi: 10.1053/j.gastro.2017.09.008. PubMed PMID: 28923495; PubMed Central PMCID: PMCPMC5801691.

29. Toyota A, Goto M, Miyamoto M, Nagashima Y, Iwasaki S, Komatsu T, et al. Novel protein kinase cAMP-Activated Catalytic Subunit Alpha (PRKACA) inhibitor shows anti-tumor activity in a fibrolamellar hepatocellular carcinoma model. Biochem Biophys Res Commun. 2022;621:157-61. Epub 2022/07/16. doi: 10.1016/j.bbrc.2022.07.008. PubMed PMID: 35839742.

30. Neumayer C, Ng D, Jiang CS, Qureshi A, Lalazar G, Vaughan R, et al. Oncogenic Addiction of Fibrolamellar Hepatocellular Carcinoma to the Fusion Kinase DNAJB1-PRKACA. Clin Cancer Res. 2023;29(1):271-8. doi: 10.1158/1078-0432.CCR-22-1851. PubMed PMID: 36302174; PubMed Central PMCID: PMCPMC9811160.

31. Cao B, Lu TW, Martinez Fiesco JA, Tomasini M, Fan L, Simon SM, et al. Structures of the PKA RIalpha Holoenzyme with the FLHCC Driver J-PKAcalpha or Wild-Type PKAcalpha. Structure. 2019;27(5):816-28 e4. Epub 2019/03/25. doi: 10.1016/j.str.2019.03.001. PubMed PMID: 30905674; PubMed Central PMCID: PMCPMC6506387.

32. Lu TW, Aoto PC, Weng JH, Nielsen C, Cash JN, Hall J, et al. Structural analyses of the PKA RIIbeta holoenzyme containing the oncogenic DnaJB1-PKAc fusion protein reveal protomer asymmetry and fusion-induced allosteric perturbations in fibrolamellar hepatocellular carcinoma. PLoS Biol. 2020;18(12):e3001018. Epub 2020/12/29. doi: 10.1371/journal.pbio.3001018. PubMed PMID: 33370777; PubMed Central PMCID: PMCPMC7793292.

33. Olivieri C, Walker C, Karamafrooz A, Wang Y, Manu VS, Porcelli F, et al. Defective internal allosteric network imparts dysfunctional ATP/substrate-binding cooperativity in oncogenic chimera of protein kinase A. Commun Biol. 2021;4(1):321. Epub 2021/03/12. doi: 10.1038/s42003-021-01819-6. PubMed PMID: 33692454; PubMed Central PMCID: PMCPMC7946884.

34. Zhang JZ, Lu TW, Stolerman LM, Tenner B, Yang JR, Zhang JF, et al. Phase Separation of a PKA Regulatory Subunit Controls cAMP Compartmentation and Oncogenic Signaling. Cell. 2020;182(6):1531-44 e15. Epub 2020/08/28. doi: 10.1016/j.cell.2020.07.043. PubMed PMID: 32846158; PubMed Central PMCID: PMCPMC7502557.

35. Turnham RE, Smith FD, Kenerson HL, Omar MH, Golkowski M, Garcia I, et al. An acquired scaffolding function of the DNAJ-PKAc fusion contributes to oncogenic signaling in fibrolamellar

524 carcinoma. Elife. 2019;8. Epub 2019/05/08. doi: 10.7554/eLife.44187. PubMed PMID: 31063128;
525 PubMed Central PMCID: PMCPMC6533061.

526 36. Piette BL, Alerasool N, Lin ZY, Lacoste J, Lam MHY, Qian WW, et al. Comprehensive
527 interactome profiling of the human Hsp70 network highlights functional differentiation of J
528 domains. Mol Cell. 2021;81(12):2549-65 e8. Epub 2021/05/07. doi:
529 10.1016/j.molcel.2021.04.012. PubMed PMID: 33957083.

530 37. Trankenschuh W, Puls F, Christgen M, Albat C, Heim A, Poczkaj J, et al. Frequent and
531 distinct aberrations of DNA methylation patterns in fibrolamellar carcinoma of the liver. PLoS One.
532 2010;5(10):e13688. Epub 2010/11/10. doi: 10.1371/journal.pone.0013688. PubMed PMID:
533 21060828; PubMed Central PMCID: PMCPMC2966398.

534 38. Dinh TA, Sritharan R, Smith FD, Francisco AB, Ma RK, Bunaciu RP, et al. Hotspots of
535 Aberrant Enhancer Activity in Fibrolamellar Carcinoma Reveal Candidate Oncogenic Pathways
536 and Therapeutic Vulnerabilities. Cell Rep. 2020;31(2):107509. Epub 2020/04/16. doi:
537 10.1016/j.celrep.2020.03.073. PubMed PMID: 32294439; PubMed Central PMCID:
538 PMCPMC7474926.

539 39. El Dika I, Bowman AS, Berger MF, Capanu M, Chou JF, Benayed R, et al. Molecular
540 profiling and analysis of genetic aberrations aimed at identifying potential therapeutic targets in
541 fibrolamellar carcinoma of the liver. Cancer. 2020;126(18):4126-35. Epub 2020/07/15. doi:
542 10.1002/cncr.32960. PubMed PMID: 32663328.

543 40. Kannangai R, Vivekanandan P, Martinez-Murillo F, Choti M, Torbenson M. Fibrolamellar
544 carcinomas show overexpression of genes in the RAS, MAPK, PIK3, and xenobiotic degradation
545 pathways. Hum Pathol. 2007;38(4):639-44. Epub 2007/03/21. doi:
546 10.1016/j.humpath.2006.07.019. PubMed PMID: 17367606.

547 41. Hirsch TZ, Pilet J, Morcrette G, Roehrig A, Monteiro BJ, Molina L, et al. Integrated genomic
548 analysis identifies driver genes and cisplatin-resistant progenitor phenotype in pediatric liver
549 cancer. Cancer Discov. 2021. Epub 2021/04/25. doi: 10.1158/2159-8290.CD-20-1809. PubMed
550 PMID: 33893148.

551 42. Dinh TA, Utria AF, Barry KC, Ma R, Abou-Alfa GK, Gordan JD, et al. A framework for
552 fibrolamellar carcinoma research and clinical trials. Nat Rev Gastroenterol Hepatol.
553 2022;19(5):328-42. Epub 2022/02/23. doi: 10.1038/s41575-022-00580-3. PubMed PMID:
554 35190728.

555 43. Dinh TA, Jewell ML, Kanke M, Francisco A, Sritharan R, Turnham RE, et al. MicroRNA-
556 375 Suppresses the Growth and Invasion of Fibrolamellar Carcinoma. Cell Mol Gastroenterol
557 Hepatol. 2019;7(4):803-17. Epub 2019/02/15. doi: 10.1016/j.jcmgh.2019.01.008. PubMed PMID:
558 30763770; PubMed Central PMCID: PMCPMC6468197.

559 44. Oikawa T, Wauthier E, Dinh TA, Selitsky SR, Reyna-Neyra A, Carpino G, et al. Model of
560 fibrolamellar hepatocellular carcinomas reveals striking enrichment in cancer stem cells. Nat
561 Commun. 2015;6:8070. Epub 2015/10/07. doi: 10.1038/ncomms9070. PubMed PMID: 26437858;
562 PubMed Central PMCID: PMCPMC4600730.

563 45. Narayan NJC, Requena D, Lalazar G, Ramos-Espiritu L, Ng D, Levin S, et al. Human liver
564 organoids for disease modeling of fibrolamellar carcinoma. Stem Cell Reports. 2022. Epub
565 2022/07/09. doi: 10.1016/j.stemcr.2022.06.003. PubMed PMID: 35803261.

566 46. Ruland L, Andreatta F, Massalini S, Chuva de Sousa Lopes S, Clevers H, Hendriks D, et
567 al. Organoid models of fibrolamellar carcinoma mutations reveal hepatocyte transdifferentiation
568 through cooperative BAP1 and PRKAR2A loss. Nat Commun. 2023;14(1):2377. Epub 20230503.

569 doi: 10.1038/s41467-023-37951-6. PubMed PMID: 37137901; PubMed Central PMCID:
570 PMCPMC10156813.

571 47. Weiel JJ, Forgo B, Sage J, Rangaswami A, Hazard FK. The Use of Fluorescence in situ
572 Hybridization to Confirm PRKACA Gene Rearrangement in Fibrolamellar Hepatocellular
573 Carcinoma: A Validation Study. Ann Clin Lab Sci. 2022;52(3):475-83. PubMed PMID: 35777788.

574 48. Walesky C, Apte U. Role of hepatocyte nuclear factor 4alpha (HNF4alpha) in cell
575 proliferation and cancer. Gene Expr. 2015;16(3):101-8. Epub 2015/02/24. doi:
576 10.3727/105221615X14181438356292. PubMed PMID: 25700366; PubMed Central PMCID:
577 PMCPMC5841246.

578 49. Sorrentino G, Rezakhani S, Yildiz E, Nuciforo S, Heim MH, Lutolf MP, et al. Mechano-
579 modulatory synthetic niches for liver organoid derivation. Nature communications. 2020;11(1):1-
580 10.

581 50. Ye S, Boeter JW, Mihajlovic M, van Steenbeek FG, van Wolferen ME, Oosterhoff LA, et
582 al. A chemically defined hydrogel for human liver organoid culture. Advanced functional materials.
583 2020;30(48):2000893.

584 51. Wells RG. The role of matrix stiffness in regulating cell behavior. Hepatology.
585 2008;47(4):1394-400.

586 52. Kozlowski MT, Crook CJ, Ku HT. Towards organoid culture without Matrigel.
587 Communications biology. 2021;4(1):1-15.

588 53. Loessner D, Meinert C, Kaemmerer E, Martine LC, Yue K, Levett PA, et al.
589 Functionalization, preparation and use of cell-laden gelatin methacryloyl–based hydrogels as
590 modular tissue culture platforms. Nature protocols. 2016;11(4):727-46.

591 54. Unagolla JM, Jayasuriya AC. Recent advances in organoid engineering: A comprehensive
592 review. Applied Materials Today. 2022;29:101582.

593 55. Teitelbaum DH, Tuttle S, Carey LC, Clausen KP. Fibrolamellar carcinoma of the liver.
594 Review of three cases and the presentation of a characteristic set of tumor markers defining this
595 tumor. Ann Surg. 1985;202(1):36-41. doi: 10.1097/00000658-198507000-00005. PubMed PMID:
596 2409935; PubMed Central PMCID: PMCPMC1250833.

597 56. Malaguarnera G, Giordano M, Paladina I, Rando A, Uccello M, Basile F, et al. Markers of
598 bile duct tumors. World Journal of Gastrointestinal Oncology. 2011;3(4):49.

599 57. Zhang L, Frank R, Furth EE, Ziober AF, LiVolsi VA, Zhang PJ. Expression and diagnostic
600 values of calretinin and CK5/6 in cholangiocarcinoma. Experimental hematology & oncology.
601 2014;3(1):1-9.

602 58. McDonald JD, Gupta S, Shindorf ML, Gamble LA, Ruff SM, Drake J, et al. Elevated serum
603 α-fetoprotein is associated with abbreviated survival for patients with fibrolamellar hepatocellular
604 carcinoma who undergo a curative resection. Annals of surgical oncology. 2020;27:1900-5.

605 59. Okuda K. Natural history of hepatocellular carcinoma including fibrolamellar and hepato-
606 cholangiocarcinoma variants. Journal of gastroenterology and hepatology. 2002;17(4):401-5.

607 60. Ferguson KM, Gillen SL, Chaytor L, Poon E, Marcos D, Gomez RL, et al. Palbociclib
608 releases the latent differentiation capacity of neuroblastoma cells. Dev Cell. 2023;58(19):1967-82
609 e8. Epub 20230920. doi: 10.1016/j.devcel.2023.08.028. PubMed PMID: 37734383.

610 61. Schuler M, Dierich A, Chambon P, Metzger D. Efficient temporally controlled targeted
611 somatic mutagenesis in hepatocytes of the mouse. Genesis. 2004;39(3):167-72. doi:
612 10.1002/gene.20039. PubMed PMID: 15282742.

62. Vyas M, Hechtman JF, Zhang Y, Benayed R, Yavas A, Askan G, et al. DNAJB1-PRKACA fusions occur in oncocytic pancreatic and biliary neoplasms and are not specific for fibrolamellar hepatocellular carcinoma. Mod Pathol. 2020;33(4):648-56. Epub 20191101. doi: 10.1038/s41379-019-0398-2. PubMed PMID: 31676785; PubMed Central PMCID: PMCPMC7125037.

63. Zhang W, Xu Y, Wang X, Oikawa T, Su G, Wauthier E, et al. Fibrolamellar carcinomas-growth arrested by paracrine signals complexed with synthesized 3-O sulfated heparan sulfate oligosaccharides. Matrix Biol. 2023;121:194-216. Epub 20230702. doi: 10.1016/j.matbio.2023.06.008. PubMed PMID: 37402431.

64. Shebl B, Ng D, Lalazar G, Rosemore C, Finkelstein TM, Migler RD, et al. Targeting BCL-XL in fibrolamellar hepatocellular carcinoma. JCI Insight. 2022;7(17). Epub 20220908. doi: 10.1172/jci.insight.161820. PubMed PMID: 36073545; PubMed Central PMCID: PMCPMC9536265.

65. Leiting JL, Hernandez MC, Bergquist JR, Yonkus JA, Abdelrahman AM, Torbenson MS, et al. Therapeutic Efficacy of Temsirolimus in a Patient-derived Model of Metastatic Fibrolamellar Hepatocellular Carcinoma. In Vivo. 2023;37(5):1940-50. doi: 10.21873/invivo.13290. PubMed PMID: 37652480; PubMed Central PMCID: PMCPMC10500502.

66. Lalazar G, Requena D, Ramos-Espiritu L, Ng D, Bhola PD, de Jong YP, et al. Identification of Novel Therapeutic Targets for Fibrolamellar Carcinoma Using Patient-Derived Xenografts and Direct-from-Patient Screening. Cancer Discov. 2021;11(10):2544-63. Epub 20210614. doi: 10.1158/2159-8290.CD-20-0872. PubMed PMID: 34127480; PubMed Central PMCID: PMCPMC8734228.

67. Grzelak CA, Goddard ET, Lederer EE, Rajaram K, Dai J, Shor RE, et al. Elimination of fluorescent protein immunogenicity permits modeling of metastasis in immune-competent settings. Cancer Cell. 2022;40(1):1-2. Epub 20211202. doi: 10.1016/j.ccell.2021.11.004. PubMed PMID: 34861158; PubMed Central PMCID: PMCPMC9668376.

68. Levin SN, Tomasini MD, Knox J, Shirani M, Shebl B, Requena D, et al. Disruption of proteome by an oncogenic fusion kinase alters metabolism in fibrolamellar hepatocellular carcinoma. Sci Adv. 2023;9(25):eadg7038. Epub 20230621. doi: 10.1126/sciadv.adg7038. PubMed PMID: 37343102; PubMed Central PMCID: PMCPMC10284549.

69. DeMichele A, Clark AS, Tan KS, Heitjan DF, Gramlich K, Gallagher M, et al. CDK 4/6 inhibitor palbociclib (PD0332991) in Rb+ advanced breast cancer: phase II activity, safety, and predictive biomarker assessment. Clin Cancer Res. 2015;21(5):995-1001. Epub 2014/12/17. doi: 10.1158/1078-0432.CCR-14-2258. PubMed PMID: 25501126.

70. O'Leary B, Cutts RJ, Liu Y, Hrebien S, Huang X, Fenwick K, et al. The Genetic Landscape and Clonal Evolution of Breast Cancer Resistance to Palbociclib plus Fulvestrant in the PALOMA-3 Trial. Cancer Discov. 2018;8(11):1390-403. Epub 2018/09/13. doi: 10.1158/2159-8290.CD-18-0264. PubMed PMID: 30206110; PubMed Central PMCID: PMCPMC6368247.

71. de Oliveira S, Houseright RA, Korte BG, Huttenlocher A. DnaJ-PKAc fusion induces liver inflammation in a zebrafish model of fibrolamellar carcinoma. Dis Model Mech. 2020;13(4). Epub 20200430. doi: 10.1242/dmm.042564. PubMed PMID: 32102783; PubMed Central PMCID: PMCPMC7197716.

72. Tasic B, Hippenmeyer S, Wang C, Gamboa M, Zong H, Chen-Tsai Y, et al. Site-specific integrase-mediated transgenesis in mice via pronuclear injection. Proc Natl Acad Sci U S A. 2011;108(19):7902-7. Epub 2011/04/06. doi: 10.1073/pnas.1019507108. PubMed PMID: 21464299; PubMed Central PMCID: PMCPMC3093482.

658 73. Postic C, Shiota M, Niswender KD, Jetton TL, Chen Y, Moates JM, et al. Dual roles for
659 glucokinase in glucose homeostasis as determined by liver and pancreatic beta cell-specific gene
660 knock-outs using Cre recombinase. J Biol Chem. 1999;274(1):305-15. Epub 1998/12/29. doi:
661 10.1074/jbc.274.1.305. PubMed PMID: 9867845.

662 74. Martin M. Cutadapt removes adapter sequences from high-throughput sequencing reads.
663 EMBnet journal. 2011;17(1):10-2.

664 75. Kim D, Paggi JM, Park C, Bennett C, Salzberg SL. Graph-based genome alignment and
665 genotyping with HISAT2 and HISAT-genotype. Nat Biotechnol. 2019;37(8):907-15. Epub
666 20190802. doi: 10.1038/s41587-019-0201-4. PubMed PMID: 31375807; PubMed Central
667 PMCID: PMCPMC7605509.

668 76. Liao Y, Smyth GK, Shi W. featureCounts: an efficient general purpose program for
669 assigning sequence reads to genomic features. Bioinformatics. 2014;30(7):923-30. Epub
670 20131113. doi: 10.1093/bioinformatics/btt656. PubMed PMID: 24227677.

671 77. Love MI, Huber W, Anders S. Moderated estimation of fold change and dispersion for
672 RNA-seq data with DESeq2. Genome Biol. 2014;15(12):550. doi: 10.1186/s13059-014-0550-8.
673 PubMed PMID: 25516281; PubMed Central PMCID: PMCPMC4302049.

FIGURE 1

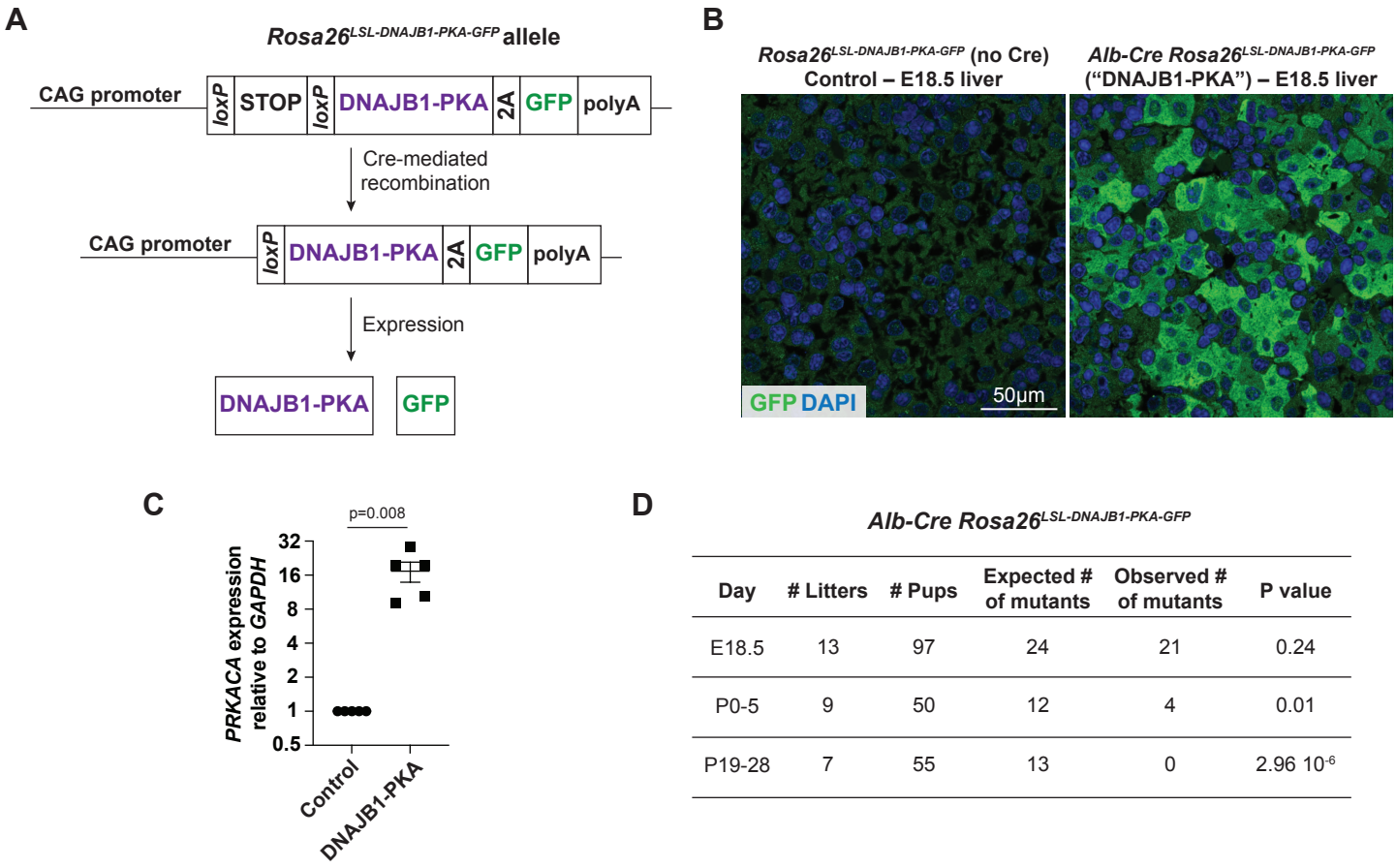

Day	# Litters	# Pups	Expected # of mutants	Observed # of mutants	P value
E18.5	13	97	24	21	0.24
P0-5	9	50	12	4	0.01
P19-28	7	55	13	0	$2.96\ 10^{-6}$

Figure 1. Generation of a transgenic mouse model to express the DNAJ1B-PRAKA fusion

A. Schematic representation of the transgene inserted into the *Rosa26* locus. The fusion cDNA is under the control of the CMV early enhancer/chicken β actin (CAG) promoter but is only expressed after Cre-mediated recombination of a transcriptional STOP cassette flanked by *loxP* sites. Upon translation, a self-cleaving 2A peptide separates the DNAJB1-PKA fusion protein from the GFP reporter. **B.** Representative confocal immunofluorescence images for GFP expression (green) from sections of control mice (transgenic mice with no Cre expression) or mice expression the fusion protein and GFP at E18.5. DAPI shows DNA staining (blue). Scale bar: 50µm. **C.** Expression levels of *PRKCA* transcripts analyzed by RT-qPCR analysis relative to *GAPDH* and to controls (n=5 E18.5 embryonic liver samples per genotype). Data shown as mean and S.E.M.; P value calculated by Mann-Whitney t-test. **D.** Analysis of expected and observed numbers of mutant mice before and after birth. P value calculated by a X^2 test.

FIGURE 2

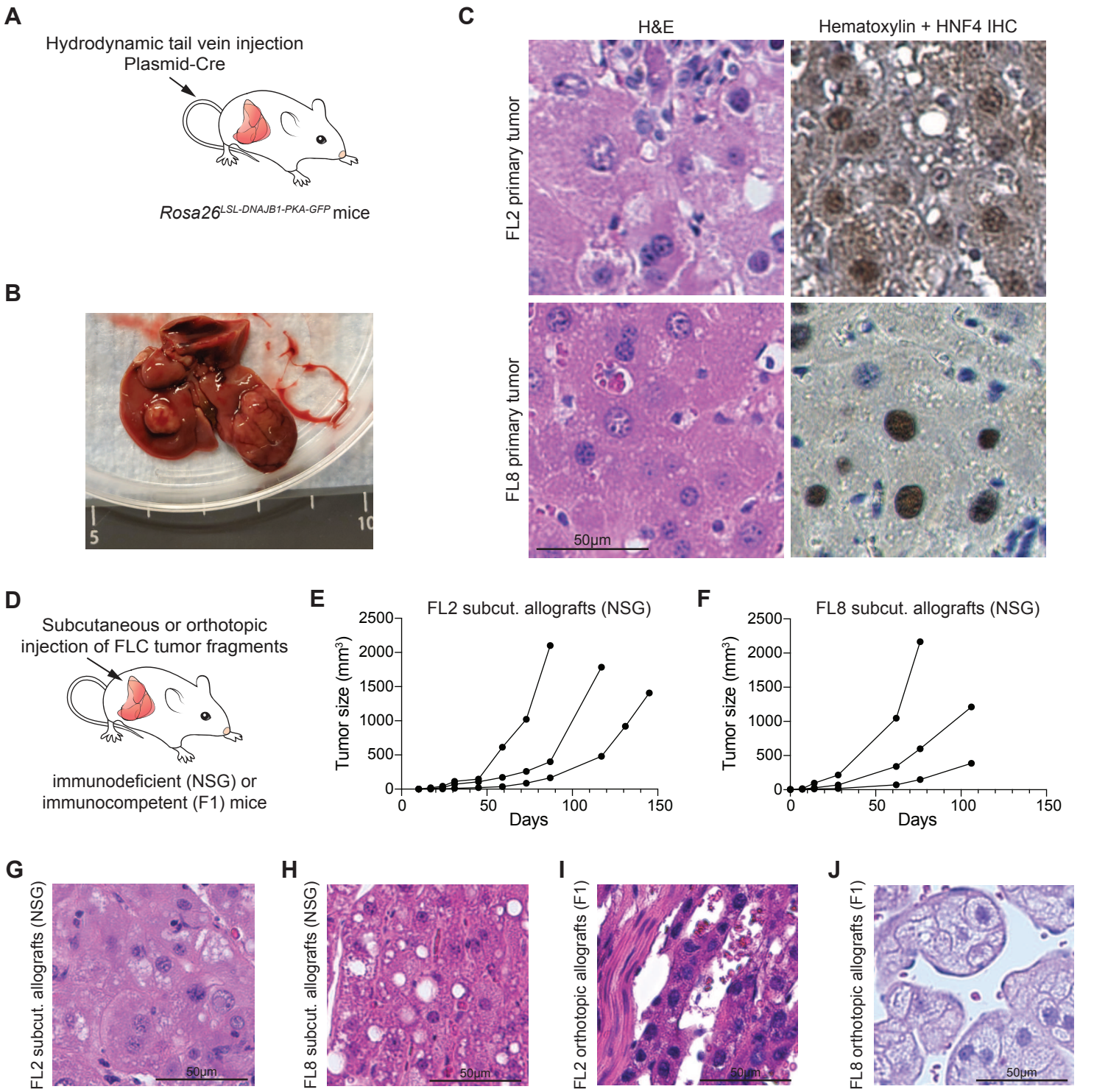

Figure 2. Propagation of tumors from transgenic mice expressing the DNAJ1B-PRAKA fusion

A. Schematic representation of the protocol to induce liver tumors in adult *Rosa26*$^{LSL\text{-}DNAJB1\text{-}PKA\text{-}GFP}$ mice upon delivery of a plasmid expressing the Cre recombinase to the liver. **B.** Representative photograph of liver tumors in the dissected liver of a *Rosa26*$^{LSL\text{-}DNAJB1\text{-}PKA\text{-}GFP}$ mouse 24.5 months after delivery of the Cre recombinase (FL1 tumor shown). **C.** Hematoxylin and eosin and hematoxylin (H&E) staining (left) and anti-HNF4α immunohistochemistry (right) on sections from the FL2 and FL8 primary tumors. Scale bar: 50µm. **D.** Schematic representation of the protocol to transplant tumor fragments from FLC models into immunodeficient or immunocompetent hosts. **E, F.** Growth of FL2 (E) and FL8 (F) subcutaneous allografts in NSG mice. **G,H**. Representative images of FL2 (G) and FL8 (H) subcutaneous allograft sections (H&E) from (E) and (F), respectively. Scale bar: 50µm. **I,J.** Representative images of FL2 (I) and FL8 (J) allograft sections (H&E) growing in the liver of C57BL/6x129Sv/J F1 immunocompetent hosts (F1). Scale bar: 50µm.

FIGURE 3

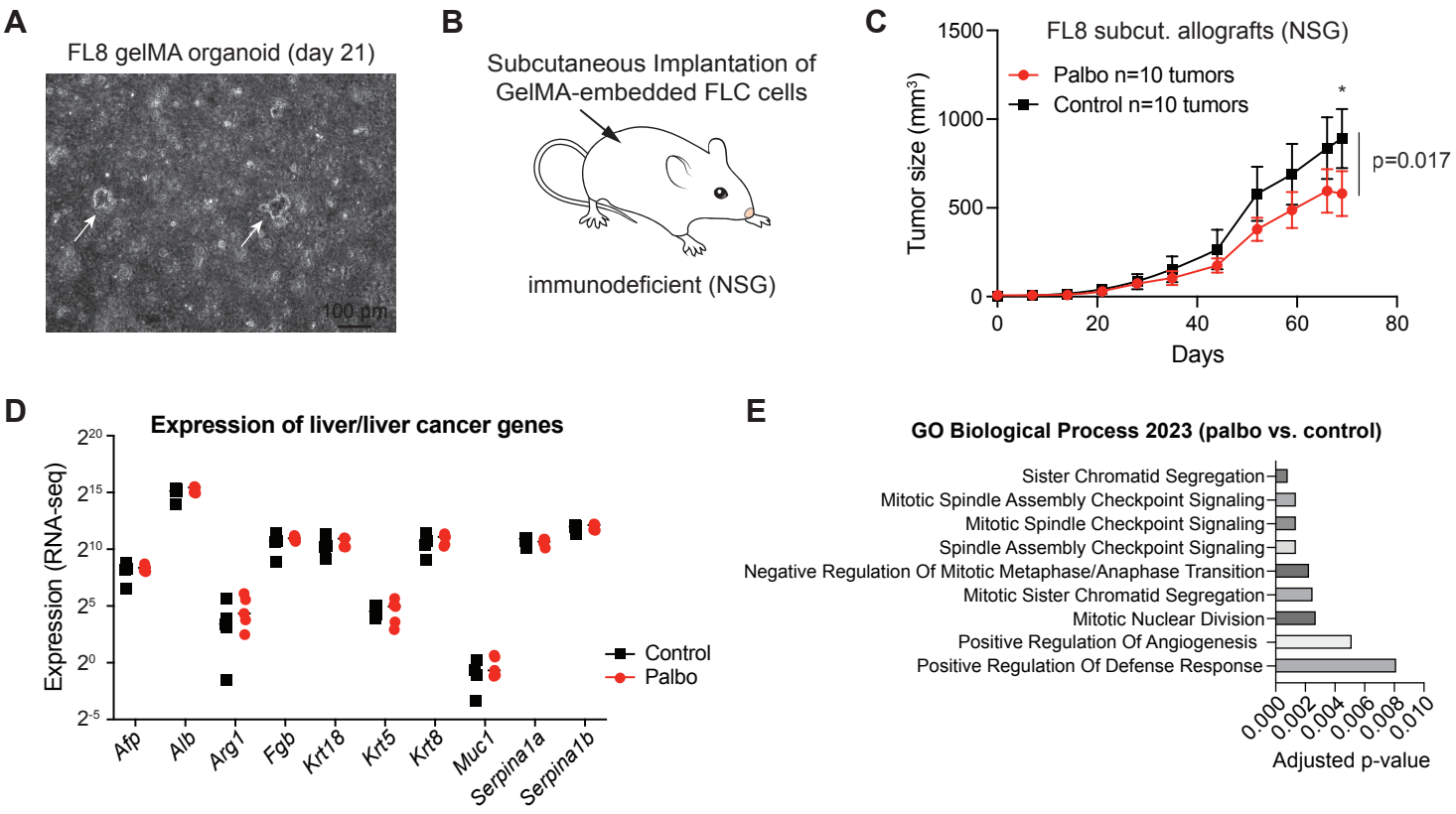

Figure 3. Inhibition of tumor growth by palbociclib

A. Representative photograph of FL8 cells growing in a GelMA matrix. Scale bar: 100µm. **B.** Schematic representation of the protocol to transplant FLC cells embedded into GelMA into immunodeficient or hosts. **C.** Growth of FL8 subcutaneous allografts treated with palbociclib (palbo) or control carrier. Data shown as mean and S.E.M.; P-value at the last time point calculated by t-test. **D.** Analysis of genes related to liver and liver cancer in control and palbociclib-treated tumors at endpoint. Data shown as mean and range. **E.** Gene Ontology (GO) analysis for biological process comparing control and palbociclib-treated tumors at endpoint.